

Laminated Graphene Films for Flexible Transparent Thin Film Encapsulation

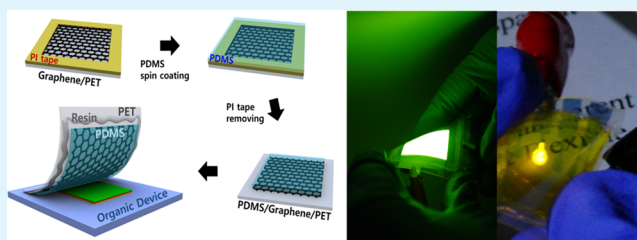
Hong-Kyu Seo, Min-Ho Park, Young-Hoon Kim, Sung-Joo Kwon, Su-Hun Jeong, and Tae-Woo Lee*

Department of Materials Science and Engineering, Pohang University of Science and Technology (POSTECH), Pohang, Gyungbuk 790-784, Republic of Korea

S Supporting Information

ABSTRACT: We introduce a simple, inexpensive, and large-area flexible transparent lamination encapsulation method that uses graphene films with polydimethylsiloxane (PDMS) buffer on polyethylene terephthalate (PET) substrate. The number of stacked graphene layers (n_G) was increased from 2 to 6, and 6-layered graphene-encapsulation showed high impermeability to moisture and air. The graphene-encapsulated polymer light emitting diodes (PLEDs) had stable operating characteristics, and the operational lifetime of encapsulated PLEDs increased as n_G increased. Calcium oxidation test data confirmed the improved impermeability of graphene-encapsulation with increased n_G . As a practical application, we demonstrated large-area flexible organic light emitting diodes (FOLEDs) and transparent FOLEDs that were encapsulated by our polymer/graphene encapsulant.

KEYWORDS: graphene, flexible lamination encapsulation, polymer light emitting diodes (PLED), lifetime, water vapor transmission rate (WVTR)



INTRODUCTION

The most representative encapsulation technology of organic electronic devices (OEDs) fabricated on a glass substrate uses a glass lid.¹ They have been encapsulated by a rigid glass lid attached by ultraviolet (UV)-curable epoxy resin in an inert atmosphere; a getter is included to absorb residual moisture and to react with molecules produced during curing of the resin and is very reliable. However, owing to the rigidity of glass encapsulant, this method is not proper for flexible OEDs.²

Thin-film encapsulation (TFE) is the most popular flexible encapsulation technique; it enables reduction in the weight and thickness of devices.^{2,3} High-density films of inorganic materials (e.g., SiN_x , SiO_x , AlO_x) that are deposited by sputtering, evaporation, or plasma vapor deposition (PVD) result in low water vapor transmission rate (WVTR).^{4–6} Multilayer stacked films are commonly used to decrease WVTR; for example, Barix encapsulation of Vitex uses stacks of inorganic and organic layer pairs made of Al_2O_3 and polyacrylate (5-dyad $\text{WVTR} < 10^{-6} \text{ g m}^{-2} \text{ d}^{-1}$).^{7,8} Another typical TFE technique can be atomic layer deposition (ALD) by which one cycle deposition terminates after the entire surface of the film has been covered; this self-limiting reaction prevents occurrence of pin holes.^{9,10} By control of film thickness and reaction cycles, ALD yields very thin and uniform barrier films at an atomic scale. These TFE methods can ensure $\text{WVTR} < 10^{-5} \text{ g m}^{-2} \text{ d}^{-1}$, but they are expensive due to the vacuum process and unproductive due to the slow rate of film growth. Furthermore, they have limitations such as the poor flexibility of inorganic films and the requirement that encapsulation be conducted at relatively low temperature to avoid damaging the OEDs.

Therefore, the feasibility of flexible OEDs could be improved by development of a simple, efficient, and inexpensive process to fabricate a highly flexible barrier film with low WVTR that can provide highly flexible encapsulation. Flexible lamination encapsulation using thin metal foils can provide one promising way to achieve these requirements¹¹ but one still needs a transparent encapsulation method for flexible OEDs which enables roll-to-roll lamination production.

Graphene^{12–14} films can provide an excellent barrier to gases or liquids due to its densely packed structure and fine carbon lattice and its thermal and chemical stability.^{15–23} Graphene is also flexible and transparent, so it has obvious potential applications as a barrier film to encapsulate flexible optoelectronics. To cover the large-area active region of an optoelectronic device, multilayered large-area graphene films are most recommended, because the layers are densely packed atop each other and can therefore minimize the number of paths by which moisture and air can cross the barrier.^{18,19} Although some reports have reported use of graphene oxide, graphene nanosheets, and composites containing them^{20–23} to prove the barrier film property of graphene, the most promising type of graphene barrier film is large-area chemical vapor deposition (CVD)-grown graphene, which has larger surface area per sheet, larger grain size, and less grain boundaries. Although gas barrier properties of CVD-grown graphene films have been demonstrated in organic photovoltaic devices

Received: February 6, 2016

Accepted: May 25, 2016

Published: June 2, 2016

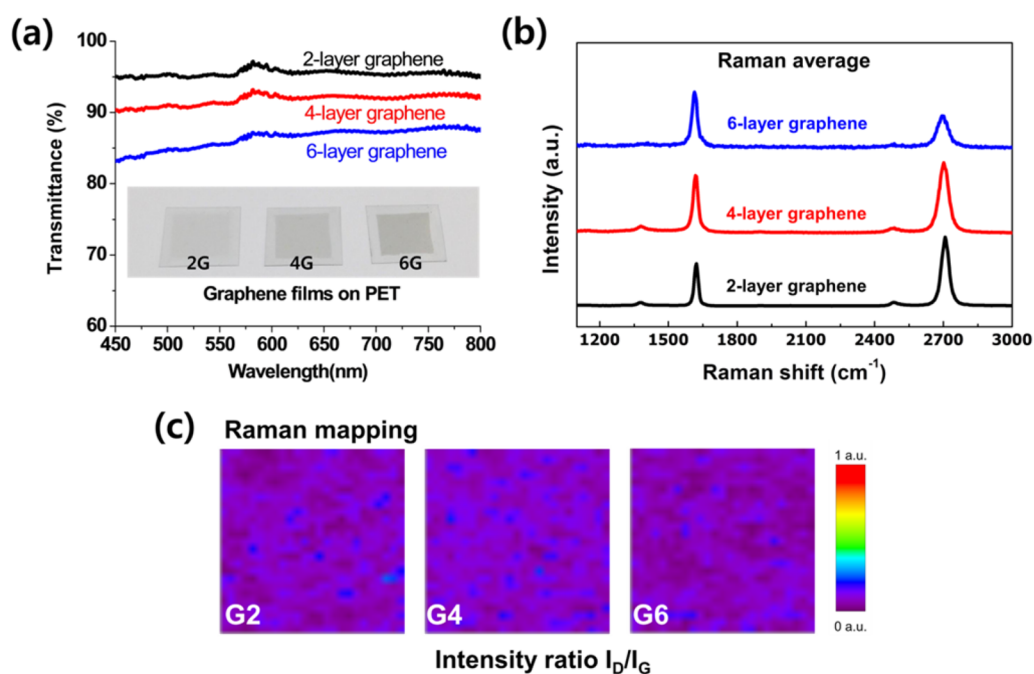


Figure 1. (a) UV-vis spectra of transferred graphene on PET substrate. Inset: image of graphene films on PET substrate, 2-, 4-, and 6-layers. (b) The average Raman spectrum ($n = 2500$ points) and (c) Raman mapping (scanned area $50 \times 50 \mu\text{m}$) of randomly stacked graphene films (G2, G4, and G6).

(OPVs) as a top electrode layer and organic field-effect transistors (OTFTs) as a top passivation layer without a reliable supporting layer,^{16,19} there have been no reports (i) to use a reliable free-standing encapsulation platform containing CVD-grown graphene barrier films which are combined with an insulating film for electrical insulation between graphene and OEDs and with a supporting substrate for reliable continuous large-scale device fabrication in a production line, and furthermore (ii) to encapsulate organic light emitting diodes (OLEDs) which are most sensitive to moisture and oxygen among OEDs.

Here, we introduce a simple, low-cost, scalable, transparent, and flexible lamination encapsulation method to encapsulate OLEDs by using multilayered CVD-grown graphene films combined with (i) an insulating and elastic polydimethylsiloxane (PDMS) buffer for insulation of graphene films from OEDs and facile lamination of graphene films on OEDs without physical damage, and (ii) a PET film as a reliable supporting substrate for the first time. The number of stacked graphene layers (n_G) was increased from 2 to 6, and 6-layered graphene-encapsulation showed high impermeability to moisture and air. The graphene-encapsulated polymer light emitting diodes (PLEDs) had stable operating characteristics, and the operational lifetime of encapsulated PLEDs increased as n_G increased. Calcium oxidation test data also confirmed the improved impermeability of graphene-encapsulation with increased n_G . Because of the flexible and transparent properties of polymer/graphene films, our graphene-encapsulation method is suitable for flexible electronic devices and for transparent display devices. As a practical application, we fabricated large-area FOLEDs (substrate area, $5 \times 5 \text{ cm}$; pixel area, $3 \times 3 \text{ cm}$) and transparent FOLEDs laminated with our polymer/graphene barrier film.

RESULTS AND DISCUSSION

To make the graphene-based encapsulation films, graphene films grown using CVD on Cu foil¹³ were transferred to a PET substrate ($2 \times 2 \text{ cm}$) by a conventional graphene transfer process.²⁴ Because the CVD-grown single-layer graphene has various defects such as pinholes, cracks, tears, and wrinkles that are generated during growth and transfer process, we used multiple-stacked graphene films to cover the defect sites.¹⁸ By repeating the transfer process, 2-layer (G2), 4-layer (G4), and 6-layer (G6) graphene films were stacked on PET (Figure 1a, inset). The multilayer graphene films showed good transparency (G6, 85.5%) at 550 nm wavelength (Figure 1a). A Raman spectroscopy system with excitation of 532 nm was used to evaluate the quality of graphene films (G2, G4, and G6).²⁵ The high quality of graphene films with few surface defects was confirmed by the average Raman spectrum (Figure 1b) and Raman mapping (D-to-G band peak intensity ratio (I_D/I_G) < 0.1) (Figure 1c).^{26,27}

Graphene is an excellent conductor, so it may cause electrical short circuits when it contacts with devices; therefore an insulating buffer layer must be inserted between the graphene-encapsulation film and the device surface. In addition, the buffer layer protects the OLEDs by absorbing external physical damage. A PDMS ($25 \mu\text{m}$) pad was formed on graphene films by spin coating and curing (Figure 2). PDMS is hydrophobic, whereas the UV-curable resin is hydrophilic; this difference in properties causes imperfect adhesion between substrate and encapsulant, and gases can penetrate through the gaps. Therefore, before spin coating of PDMS, the four-edge of graphene/PET substrate ($\sim 3 \text{ mm}$) was sealed with polyimide (PI) tape, which was removed after the PDMS-curing process to obtain the region that resin will be coated.

To utilize graphene-encapsulation, we fabricated polymer light emitting diodes (PLEDs) (Figure 3a) composed of indium tin oxide (ITO) (185 nm)/self-organized gradient hole

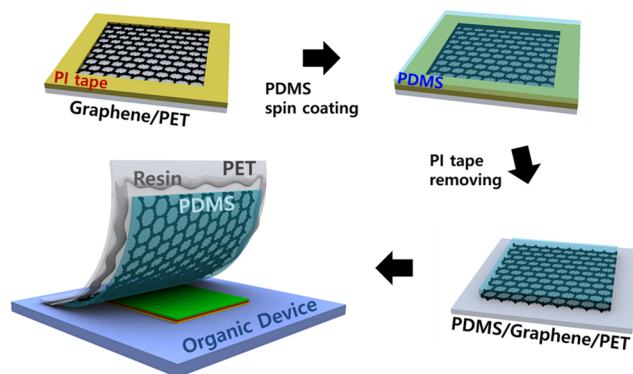


Figure 2. Schematic of graphene-encapsulation procedure.

injection layer (GraHIL) (50 nm)^{13,28}/green-emitting poly-fluorene copolymer (Dow Green-B) (80 nm)/lithium fluoride (LiF) (1 nm)/Al (110 nm) (see the [Experimental Section](#)). A graphene-encapsulation barrier (PDMS/G2/PET, PDMS/G4/PET, or PDMS/G6/PET) or a flexible encapsulation barrier without graphene (PET only or PDMS/PET) was attached to each PLED after device fabrication ([Figure 3b,c](#)). The graphene-encapsulated PLEDs showed identical electrical characteristics ([Figure 3d–f](#)). All PLEDs had similar current density ([Figure 3d](#)); this result means that graphene-encapsulated devices were well-encapsulated without any damage due to contact with the encapsulation film. The encapsulated devices turned on around 2.5 V and had identical operating voltage of around 4, 5, and 7.5 V at 100, 1000, and 10000 cd m^{-2} , respectively ([Figure 3e](#)). Current efficiency was stable and very similar in all of the devices except one that was encapsulated using only PET, which showed lower current efficiency, possibly due to incomplete encapsulation and rapid penetration of moisture and air through the PET ([Figure 3f](#)). A flat PET film without a PDMS buffer layer (25- μm -thick) lacks edge space filled with resin. Therefore, the resin can spread from the edge of the substrate to its center and then attack the pixel area.

The half-luminescence lifetimes (L_{50} , time for luminance to decline by 50% in air) of PLEDs were measured at initial

luminance of 1000 cd m^{-2} ([Figure 4](#)). L_{50} of the PLED that was exposed to the air after device fabrication (without

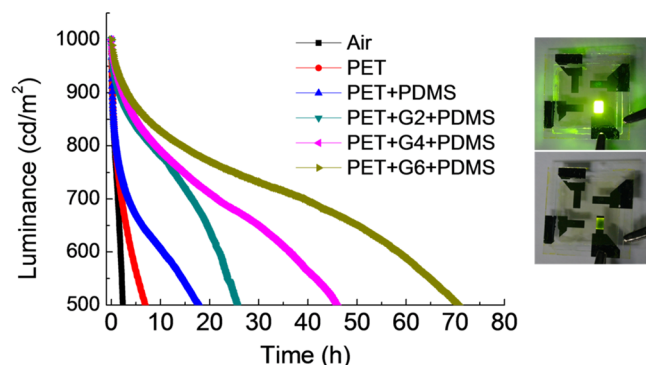


Figure 4. Luminance decay of OLEDs encapsulated using various methods. (Initial luminance, 1000 cd m^{-2}) Inset: photographs of PLED exposed to air without encapsulation (up, as exposed; down, after 3 h).

encapsulation) was only 2.3 h, and a large dark spot appeared in the pixel area after ~ 3 h ([Figure 4](#), inset). L_{50} of PLEDs increased when they were encapsulated with PET or PDMS/PET films but did not exceed 20 h, because of the relatively high permeability of PET and PDMS to moisture and air. L_{50} of the PLEDs with graphene-encapsulation layers increased as n_G increased, because this increase amplified the impermeability of graphene to moisture and air. The graphene encapsulation with $n_G = 6$ resulted in device half-lifetime of 70.7 h. The increase in lifetime had not ceased at $n_G = 6$, so additional graphene layers may further increase L_{50} of devices, but this approach would only be reasonable when loss of optical transparency is not important.

To determine the effect of graphene on the barrier film properties, we conducted a electrical Ca test to obtain WVTR, which measures the degree of Ca corrosion with high accuracy ([Figure 5](#)).^{11,29–31} Ca films (200 nm) with an area of $1.2 \text{ cm} \times 1.2 \text{ cm}$ were deposited on patterned Al electrodes on glass substrates ([Figure S1](#)), and the ensembles were encapsulated using PET, PDMS/PET, or PDMS/2, 4, 6-layer graphene/

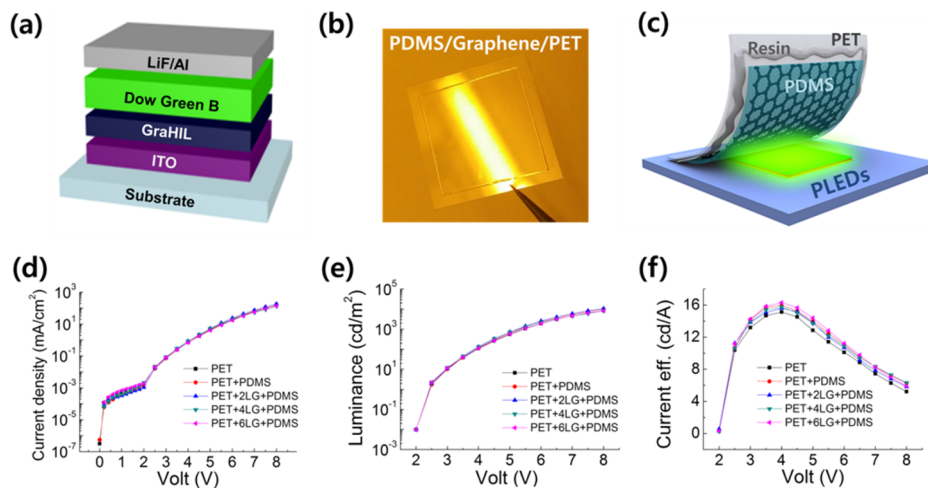


Figure 3. (a) Device structure of PLEDs for evaluating encapsulation properties. (b) Image of graphene-encapsulation film: PDMS/graphene/PET. (c) Structure of graphene-encapsulation on device substrate. (d–f) Electrical properties of encapsulated PLEDs: (d) current density–voltage, (e) luminance–voltage, and (f) current efficiency–voltage.

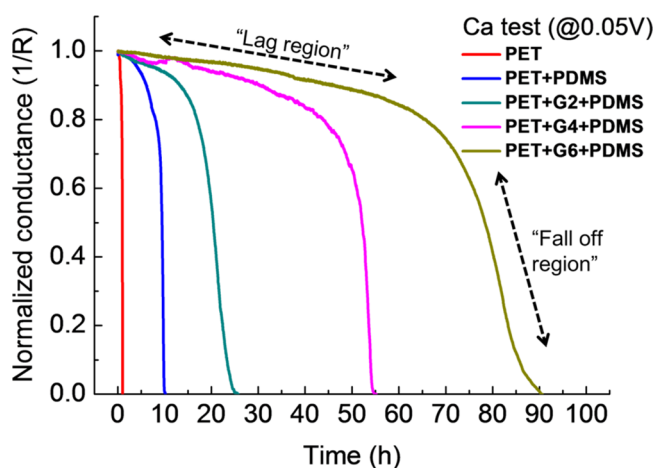


Figure 5. Normalized conductance versus time from Ca oxidation test of encapsulated Ca film at 25 °C, 45% RH, and 0.05 V. Dashed arrows: lag region (left) and fall off region (right).

PET. Water vapor passing through barrier films reacts with the metallic Ca to form insulating $\text{Ca}(\text{OH})_2$; as a result the resistance R of the film increases as the oxidation increases. The slope of normalized conductance ($C = 1/R$) versus time corresponds to WVTR ($\text{g m}^{-2} \text{d}^{-1}$) of the encapsulant:

$$\text{WVTR}(\text{g m}^{-2} \text{d}^{-1}) = -n \left(\frac{M_{\text{H}_2\text{O}}}{M_{\text{Ca}}} \right) \times \rho_{\text{Ca}} \sigma \left[\frac{d(1/R)}{dt} \right] \left(\frac{S_{\text{Ca}}}{S} \right)$$

where n ($= 2$) is the reaction ratio of the degradation, $M_{\text{H}_2\text{O}}$ and M_{Ca} are the molar masses of water ($= 18 \text{ g mol}^{-1}$) and Ca ($= 40.1 \text{ g mol}^{-1}$), ρ_{Ca} and σ are the Ca density ($= 1.54 \times 10^6 \text{ g m}^{-3}$) and resistivity ($= 3.5 \times 10^{-8} \Omega \text{ m}$), $[d(1/R)/dt]$ is the rate of the conductance change ($\Omega^{-1} \text{d}^{-1}$), (S_{Ca}/S) is the area ratio of Ca film to the aperture of the encapsulation.¹¹ Measurements were performed at 25 °C, 45% relative humidity (RH) at 0.05 V.

All plots of normalized C vs time had two major slope regions (Figure 5). In the first region, C decreased slowly with linear slope over time which is often referred to as a “lag time”.³² The initial C is nearly constant in the “lag region” due to slow vertical penetration of moisture and air through a long tortuous path of the barrier films. The sequence of points at which the C reaches zero about all samples was consistent with that of L_{50} of encapsulated PLEDs. The C of the bare PET sample collapsed rapidly (1 h) and we did not calculate the lag time at this point due to its very short lag region ($< 1 \text{ h}$) (Table 1 and Figure S2). The lag time of graphene-encapsulated sample increased as n_G increased and the film encapsulated with PDMS/G6/PET had the longest lag time ($\sim 65 \text{ h}$). This result may occur because multilayer-stacked graphene films can pack closely together with regular interlayer spacing ($\sim 0.34 \text{ nm}$).^{27,33} These multilayer stacks can patch the defects in component layers, such as point defects that are generated during graphene

synthesis, and polymer residues, ripples, macroscale cracks, and pores that are generated during metal etching, and graphene transfer.^{15,19} As a result, the graphene stacks form a defect-sealed membrane with low permeability to moisture and air (Figure 6a,b and Figure S3a,b).

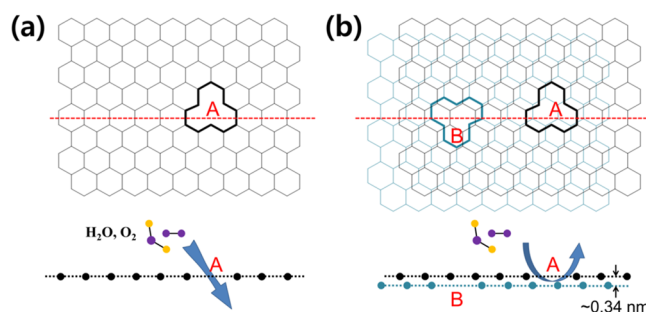


Figure 6. Schematic diagram of (a) single-layer graphene and (b) 2-layer graphene barrier films with point defects in the air (H_2O , O_2).

In the second region, the C decreased rapidly, possibly because of fast horizontal diffusion of moisture and air through the gap between the films.¹⁹ We calculated the WVTR value from the slope over the range in which C was 40–60% of the initial value in the “fall off region” (Table 1).^{34,35} The calculated WVTR value of PET in the fall off region was $2.18 \text{ g m}^{-2} \text{d}^{-1}$, which is comparable to the previously reported value.¹⁶ The WVTR value decreased significantly to $3.44 \times 10^{-1} \text{ g m}^{-2} \text{d}^{-1}$ for PDMS/PET and it decreased further as n_G increased (Figure S2). The film encapsulated with PDMS/G6/PET had the lowest WVTR in the fall off region ($1.78 \times 10^{-2} \text{ g m}^{-2} \text{d}^{-1}$) as predicted from lifetime data of encapsulated PLEDs. This value is similar to the previous report that demonstrated graphene gas-barrier films.¹⁹ Compared with the previous report, the WVTR value of PDMS/G6/PET film in the fall off region ($1.78 \times 10^{-2} \text{ g m}^{-2} \text{d}^{-1}$) is lower than that of G6/PET film in previous reported data ($4.8 \times 10^{-1} \text{ g m}^{-2} \text{d}^{-1}$, saturated region). We attribute this improved result to the additional PDMS buffer layer which can provide a sticking layer that eliminates any space in which gas can accumulate between Ca and encapsulant.

Compared with conventional TFE ($< 10^{-4} \text{ g m}^{-2} \text{d}^{-1}$), the WVTR of our graphene-encapsulation is higher. However, WVTR can be further decreased by replacing the PET to another polymer which has low penetration rate, increasing n_G , or using hybrids of graphene with additional organic or inorganic layer. Because our barrier film-making process is simple, scalable, and less expensive, it will provide a solution for overcoming the obstacles of previously reported methods to fabricate TFE when its WVTR can be reduced as low as those of conventional methods. Furthermore, because roll-to-roll transfer of large-area graphene is possible²⁶ and the buffer layer can be obtained easily on graphene by many kinds of coating process, this graphene-encapsulation method is compatible with roll-to-roll fabrication processes, which have high throughput

Table 1. Calculated Lag Times and WVTR Values of Several Encapsulants^a

	PET	PET + PDMS	PET + G2 + PDMS	PET + G4 + PDMS	PET + G6 + PDMS
lag time (h)	–	7	13	45	65
WVTR ($\text{g m}^{-2} \text{d}^{-1}$)	2.18	$3.44 \times 10^{-1} (\pm 1 \times 10^{-2})$	$5.52 \times 10^{-2} (\pm 3 \times 10^{-4})$	$3.93 \times 10^{-2} (\pm 6 \times 10^{-4})$	$1.78 \times 10^{-2} (\pm 9 \times 10^{-5})$

^aLag times and WVTR values were calculated on lag and fall off regions of Ca test plot, respectively.

and large-area production and can therefore reduce manufacturing cost.

To demonstrate the practical use of our graphene-encapsulation in flexible device application, we fabricated large-area FOLED that was encapsulated using our method (Figure 7a). The large-area FOLED on an ITO-coated PET

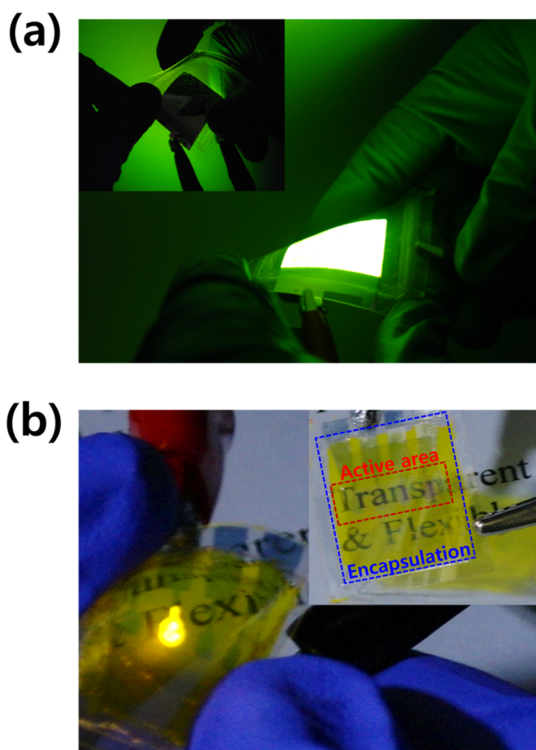


Figure 7. (a) Demonstration of large-area FOLEDs on ITO coated PET substrate with flexible encapsulation using graphene-encapsulation film in the air condition. (Substrate area, 5 cm \times 5 cm; pixel area, 3 cm \times 3 cm) Inset: encapsulated-side which shows Al cathode (top-side). (b) Demonstration of transparent FOLEDs on ITO coated PET substrate with flexible encapsulation using graphene-encapsulation film in the air conditions. Inset: turn off state.

substrate (substrate area, 5 cm \times 5 cm; pixel area, 3 cm \times 3 cm) with the same structure that we used before (Figure 3a) was encapsulated using PET/G6/PDMS (4 cm \times 4 cm), and showed stable operation with uniform light emission in air, while in a highly bent state. We also fabricated a transparent FOLED (ITO (100 nm)/ZnO (22 nm)/polyethylenimine ethoxylated (PEIE) (8 nm)/Super Yellow (230 nm)/MoO₃ (5 nm)/Ag (15 nm)/MoO₃ (45 nm))³⁶ (see the Experimental Section) that emits light toward the bottom and top (encapsulated) side; this device demonstrates that our flexible transparent encapsulation can be applied to transparent or top-emitting flexible display devices (Figure 7b).

CONCLUSIONS

We demonstrated a simple, low-cost, scalable, transparent, and flexible lamination encapsulation for OLEDs by using multi-stacked graphene films with a PDMS buffer on a PET substrate. The electrical and electro-optical characteristics of graphene-encapsulated OLEDs showed stable operation upon encapsulation, and the operational lifetime of OLEDs indicated that the permeability of our graphene-encapsulation decreased as the number of graphene layers increased. A Ca oxidation test

confirmed this conclusion. We fabricated large-area and transparent FOLEDs with our graphene-encapsulation method, which maximizes the merits of flexible transparent graphene encapsulation. We believe that after further optimization, this graphene-encapsulation method can eventually achieve a flexible and highly impermeable encapsulant that overcomes drawbacks of glass encapsulation and typical TFE such as rigid, expensive, and unproductive processes and the impossibility of roll-to-roll. We also believe that our work shows the great potential of the new flexible encapsulation method to be applied in flexible OEDs such as OTFTs, OPVs, and OLEDs, which provide a barrier to moisture and air that is comparable in impermeability to the conventional flexible encapsulant.

EXPERIMENTAL SECTION

PDMS Buffer Layer. PDMS solution (silicone elastomer base, curing agent = 10 wt/1 wt, SYLGARD 184, Dow Corning) was prepared, then the bubbles in PDMS solution were removed by using a vacuum desiccator for 30 min. The edge of graphene/PET substrates (\sim 3 mm) was sealed with polyimide tape (PI) before spin coating. The PDMS solution was spin coated on the graphene/PET (2 cm \times 2 cm) substrates at 1000 rpm for 1 min. The PDMS/graphene/PET was annealed for 1 h at 80 $^{\circ}$ C for PDMS curing, then PI tape was removed. Finally, the PDMS/graphene/PET substrate was laminated and encapsulated by using a UV-curable epoxy resin (XNR5570, Nagase ChemteX Corporation) on PLEDs. In the case of large-area FOLED, typical epoxy adhesive (Araldite, Huntsman Corporation) was used for PDMS/graphene/PET (4 cm \times 4 cm) encapsulant.

PLED (and FOLED) Fabrication. A patterned ITO (work function \sim 4.8 eV, 185 nm) on a glass substrate (2.5 cm \times 2.5 cm) (an ITO film (100 nm) on a PET substrate (5 cm \times 5 cm) in the case of large-area FOLED) was used as an anode. The pixel area of PLEDs was 6 mm² (9 cm² in the case of large-area FOLED). ITO coated anodes were cleaned by sonication with acetone and isopropyl alcohol (IPA) and then dried on a hot plate. UV–ozone was treated for 15 min, then a GraHIL^{13,28} solution, composed of PEDOT/PSS (poly(3,4-ethylenedioxythiophene) doped with poly(styrenesulfonate), Clevis P VP AI4083) and tetrafluoroethylene-perfluoro-3,6-dioxo-4-methyl-7-octene-sulfonic acid copolymer (one of the perfluorinated ionomers, CAS Number: 31175-20-9, Sigma-Aldrich) in a 1:1 ratio, was spin coated on the ITO anodes in air at 4500 rpm for 90 s. After GraHIL spin coating, samples were annealed immediately on a hot plate in air at 150 $^{\circ}$ C for 30 min, then loaded in a N₂ glovebox. Green-emitting polyfluorene copolymer (80 nm, Dow LUMATION Green-B, Dow Chemical Co.), as an emitting layer was spin coated on GraHIL at 3000 rpm for 90 s and annealed on a hot plate at 85 $^{\circ}$ C for 20 min under N₂ in a glovebox, then loaded in a high vacuum chamber (5×10^{-7} Torr). Cathode layers of LiF (1 nm)/Al (110 nm) were vacuum deposited.

Transparent FOLED Fabrication. PET substrates (2.5 cm \times 2.5 cm) coated with ITO (100 nm) were used for PLED fabrication. The pixel area of PLEDs was 4 mm². After substrate cleaning, ZnO (22 nm) was spin coated on ITO substrate at 1000 rpm for 60 s and immediately annealed on a hot plate for 1 h at 150 $^{\circ}$ C. PEIE solution (8 nm, dissolved in 2-methoxyethanol) was spin coated on ZnO layer at 5000 rpm for 90 s and annealed on a hot plate for 10 min at 100 $^{\circ}$ C, then loaded in a N₂ glovebox. A Super Yellow (230 nm, Merck OLED Materials, GmbH, catalog number PDY-132) emitting layer was spin coated on the PEIE layer at 5000 rpm for 90 s and annealed on a hot plate for 20 min at 80 $^{\circ}$ C in a N₂ glovebox, then loaded in a high vacuum chamber (5×10^{-7} Torr).³⁶ MoO₃ (5 nm)/Ag (15 nm)/MoO₃ (45 nm) were vacuum deposited as a HIL and transparent cathode.

OLED Characterization. The electro-optical characteristics of encapsulated PLEDs were measured by a source-measurement unit (Keithley 236) and a spectroradiometer (Minolta CS2000). Lifetimes of PLEDs were measured by using Polaronix M6000 (McScience) at 25 $^{\circ}$ C and 45% RH.

WVTR Measurement. The WVTR was measured by using Polaronix M6000 (McScience) with Ca film (200 nm, Sigma-Aldrich) at 25 °C and 45% RH.

■ ASSOCIATED CONTENT

Supporting Information

The Supporting Information is available free of charge on the ACS Publications website at DOI: 10.1021/acsami.6b01639.

Lag times and WVTR values calculated on lag and fall off regions of the Ca test plot, atomic force microscopy (AFM) and optical microscope images of several defects on single-layer graphene (PDF)

■ AUTHOR INFORMATION

Corresponding Author

*E-mail: twlee@postech.ac.kr, taewlees@gmail.com.

Notes

The authors declare no competing financial interest.

■ ACKNOWLEDGMENTS

This work was supported by the National Research Foundation of Korea (NRF) grant funded by the Korea government (Grant NRF-2013R1A2A2A01068753) and the Ministry of Science, ICT and Future Planning (MSIP), Korea, under the "IT Consilience Creative Program" (Grant IITP-2015-R0346-15-1007).

■ REFERENCES

- (1) Burrows, P. E.; Bulovic, V.; Forrest, S. R.; Sapochak, L. S.; McCarty, D. M.; Thompson, M. E. Reliability and Degradation of Organic Light Emitting Devices. *Appl. Phys. Lett.* **1994**, *65*, 2922–2924.
- (2) Park, M. H.; Han, T. H.; Kim, Y. H.; Jeong, S. H.; Lee, Y.; Seo, H. K.; Cho, H.; Lee, T.-W. Flexible organic light-emitting diodes for solid-state lighting. *J. Photonics Energy* **2015**, *5*, 053599.
- (3) Ghosh, A. P.; Gerenser, L. J.; Jarman, C. M.; Fornalik, J. E. Thin-Film Encapsulation of Organic Light-Emitting Devices. *Appl. Phys. Lett.* **2005**, *86*, 223503.
- (4) da Silva Sobrinho, A. S.; Latreche, M.; Czeremuskin, G.; Klemberg-Sapieha, J. E.; Wertheimer, M. R. Transparent Barrier Coatings on Polyethylene Terephthalate by Single- and Dual-Frequency Plasma-Enhanced Chemical Vapor Deposition. *J. Vac. Sci. Technol., A* **1998**, *16*, 3190–3198.
- (5) Lueder, E. Passive and Active Matrix Liquid Crystal Displays with Plastic Substrates. *Proc. Electrochem. Soc.* **1999**, *98*, 336–354.
- (6) Henry, B. M.; Dinelli, F.; Zhao, K. Y.; Grovenor, C. R. M.; Kolosov, O. V.; Briggs, G. A. D.; Roberts, A. P.; Kumar, R. S.; Howson, R. P. A Microstructural Study of Transparent Metal Oxide Gas Barrier Films. *Thin Solid Films* **1999**, *355–356*, 500–504.
- (7) Tropsha, T. G.; Harvey, N. G. Activated Rate Theory Treatment of Oxygen and Water Transport through Silicon Oxide/Poly(ethylene terephthalate) Composite Barrier Structures. *J. Phys. Chem. B* **1997**, *101*, 2259–2266.
- (8) Weaver, M. S.; Michalski, L. A.; Rajan, K.; Rothman, M. A.; Silvernail, J. A.; Brown, J. J.; Burrows, P. E.; Graff, G. L.; Gross, M. E.; Martin, P. M.; Hall, M.; Mast, E.; Bonham, C.; Bennett, W.; Zumhoff, M. Organic Light-Emitting Devices with Extended Operating Lifetimes on Plastic Substrates. *Appl. Phys. Lett.* **2002**, *81*, 2929–2931.
- (9) Dameron, A. A.; Davidson, S. D.; Burton, B. B.; Carcia, P. F.; McLean, R. S.; George, S. M. Gas Diffusion Barriers on Polymers using Multilayers fabricated by Al₂O₃ and Rapid SiO₂ Atomic Layer Deposition. *J. Phys. Chem. C* **2008**, *112*, 4573–4580.
- (10) Lee, B. H.; Yoon, B.; Anderson, V. R.; George, S. M. Alucone Alloys with Tunable Properties using Alucone Molecular Layer

Deposition and Al₂O₃ Atomic Layer Deposition. *J. Phys. Chem. C* **2012**, *116*, 3250–3257.

(11) Park, M.-H.; Kim, J.-Y.; Han, T.-H.; Kim, T.-S.; Kim, H.; Lee, T.-W. Flexible Lamination Encapsulation. *Adv. Mater.* **2015**, *27*, 4308–4314.

(12) Geim, A. K.; Novoselov, K. S. The Rise of Graphene. *Nat. Mater.* **2007**, *6*, 183–191.

(13) Han, T.-H.; Lee, Y.; Choi, M.-R.; Woo, S.-H.; Bae, S.-H.; Hong, B. H.; Ahn, J.-H.; Lee, T.-W. Extremely Efficient Flexible Organic Light-Emitting Diodes with Modified Graphene Anode. *Nat. Photonics* **2012**, *6*, 105–110.

(14) Byun, S.-J.; Lim, H.; Shin, G.-Y.; Han, T.-H.; Oh, S. H.; Ahn, J.-H.; Choi, H. C.; Lee, T.-W. Graphenes Converted from Polymers. *J. Phys. Chem. Lett.* **2011**, *2*, 493–497.

(15) Bunch, J. S.; Verbridge, S. S.; Alden, J. S.; van der Zande, A. M.; Parpia, J. M.; Craighead, H. G.; McEuen, P. L. Impermeable Atomic Membranes from Graphene Sheets. *Nano Lett.* **2008**, *8*, 2458–2462.

(16) Liu, Z.; Li, J.; Yan, F. Package-Free Flexible Organic Solar Cells with Graphene Top Electrodes. *Adv. Mater.* **2013**, *25*, 4296–4301.

(17) Zhao, Y.; Xie, Y.; Hui, Y. Y.; Tang, L.; Jie, W.; Jiang, Y.; Xu, L.; Lau, S. P.; Chai, Y. Highly Impermeable and Transparent Graphene as an Ultra-Thin Protection Barrier for Ag Thin Films. *J. Mater. Chem. C* **2013**, *1*, 4956–4961.

(18) Boutilier, M. S. H.; Sun, C.; O'Hern, S. C.; Au, H.; Hadjiconstantinou, N. G.; Karnik, R. Implications of Permeation through Intrinsic Defects in Graphene on the Design of Defect-Tolerant Membranes for Gas Separation. *ACS Nano* **2014**, *8*, 841–849.

(19) Choi, K.; Nam, S.; Lee, Y.; Lee, M.; Jang, J.; Kim, S. J.; Jeong, Y. J.; Kim, H.; Bae, S.; Yoo, J.-B.; Cho, S. M.; Choi, J.-B.; Chung, H. K.; Ahn, J.-H.; Park, C. E.; Hong, B. H. Reduced Water Vapor Transmission Rate of Graphene Gas Barrier Films for Flexible Organic Field-Effect Transistors. *ACS Nano* **2015**, *9*, 5818–5824.

(20) Su, Y.; Kravets, V. G.; Wong, S. L.; Waters, J.; Geim, A. K.; Nair, R. R. Impermeable Barrier Films and Protective Coatings Based on Reduced Graphene Oxide. *Nat. Commun.* **2014**, *5*, 4843.

(21) Yamaguchi, H.; Granstrom, J.; Nie, W.; Sojoudi, H.; Fujita, T.; Voiry, D.; Chen, M.; Gupta, G.; Mohite, A. D.; Graham, S. Reduced Graphene Oxide Thin Films as Ultrabarrriers for Organic Electronics. *Adv. Energy Mater.* **2014**, *4*, 1300986.

(22) Tseng, I.-H.; Liao, Y.-F.; Chiang, J.-C.; Tsai, M.-H. Transparent Polyimide/Graphene Oxide Nanocomposite with Improved Moisture Barrier Property. *Mater. Chem. Phys.* **2012**, *136*, 247–253.

(23) Lee, S.; Hong, J. Y.; Jang, J. Multifunctional Graphene Sheets Embedded in Silicone Encapsulant for Superior Performance of Light-Emitting Diodes. *ACS Nano* **2013**, *7*, 5784–5790.

(24) Li, X. S.; Zhu, Y. W.; Cai, W. W.; Borysiak, M.; Han, B. Y.; Chen, D.; Piner, R. D.; Colombo, L.; Ruoff, R. S. Transfer of Large-Area Graphene Films for High-Performance Transparent Conductive Electrodes. *Nano Lett.* **2009**, *9*, 4359–4363.

(25) Ferrari, A. C.; Meyer, J. C.; Scardaci, V.; Casiraghi, C.; Lazzeri, M.; Mauri, F.; Piscanec, S.; Jiang, D.; Novoselov, K. S.; Roth, S.; Geim, A. K. Raman Spectrum of Graphene and Graphene Layers. *Phys. Rev. Lett.* **2006**, *97*, 187401.

(26) Bae, S.; Kim, H.; Lee, Y.; Xu, X.; Park, J. S.; Zheng, Y.; Balakrishnan, J.; Lei, T.; Kim, H. R.; Song, Y. I. Roll-to-Roll Production of 30-Inch Graphene Films for Transparent Electrodes. *Nat. Nanotechnol.* **2010**, *5*, 574–578.

(27) Seo, H.-K.; Kim, T.-S.; Park, C.; Xu, W.; Baek, K.; Bae, S.-H.; Ahn, J.-H.; Kim, K.; Chio, H. C.; Lee, T.-W. Value-added Synthesis of Graphene: Recycling Industrial Carbon Waste into Electrodes for High-Performance Electronic Devices. *Sci. Rep.* **2015**, *5*, 16710.

(28) Lee, T.-W.; Chung, Y.; Kwon, O.; Park, J.-J. Self-Organized Gradient Hole Injection to Improve the Performance of Polymer Electroluminescent Devices. *Adv. Funct. Mater.* **2007**, *17*, 390–396.

(29) Park, J. S.; Chae, H.; Chung, H. K.; Lee, S. I. Thin Film Encapsulation for Flexible AM-OLED: a Review. *Semicond. Sci. Technol.* **2011**, *26*, 034001.

(30) Paetzold, R.; Winnacker, A.; Henseler, D.; Cesari, V.; Heuser, K. Permeation Rate Measurements by Electrical Analysis of Calcium Corrosion. *Rev. Sci. Instrum.* **2003**, *74*, 5147–5150.

(31) Choi, J. H.; Kim, Y. M.; Park, Y. W.; Huh, J. W.; Kim, I. S.; Hwang, H. N.; Ju, B. K. Evaluation of Gas Permeation Barrier Properties using Electrical Measurements of Calcium Degradation. *Rev. Sci. Instrum.* **2007**, *78*, 064701.

(32) Graff, G. L.; Williford, R. E.; Burrows, P. E. Mechanisms of Vapor Permeation Through Multilayer Barrier Films: Lag Time versus Equilibrium Permeation. *J. Appl. Phys.* **2004**, *96*, 1840–1849.

(33) Kim, K. S.; Zhao, Y.; Jang, H.; Lee, S. Y.; Kim, J. M.; Kim, K. S.; Ahn, J. H.; Kim, P.; Choi, J. Y.; Hong, B. H. Large-Scale Pattern Growth of Graphene Films for Stretchable Transparent Electrodes. *Nature* **2009**, *457*, 706–710.

(34) Zhang, S.; Xue, W.; Yu, Z. Moisture Barrier Evaluation of SiO_x/SiN_x Stacks on Polyimide Substrates using Electrical Calcium Test. *Thin Solid Films* **2015**, *580*, 101–105.

(35) Seo, S.-W.; Jung, E.; Lim, C.; Chae, H.; Cho, S. M. Water Permeation through Organic–Inorganic Multilayer Thin Films. *Thin Solid Films* **2012**, *520* (21), 6690–6694.

(36) Kim, Y. H.; Han, T. H.; Cho, H.; Min, S. Y.; Lee, C. L.; Lee, T. W. Polyethylene Imine as an Ideal Interlayer for Highly Efficient Inverted Polymer Light-Emitting Diodes. *Adv. Funct. Mater.* **2014**, *24*, 3808–3814.